MCB Journals.ASM.org

Pknox1/Prep1 Regulates Mitochondrial Oxidative Phosphorylation Components in Skeletal Muscle

Timo Kanzleiter,[a,e] Michaela Rath,[a,e] Dmitry Penkov,[b,c] Dmytro Puchkov,[d] Nadja Schulz,[a,e] Francesco Blasi,[b] Annette Schürmann[a,e]

Department of Experimental Diabetology, German Institute of Human Nutrition, Potsdam-Rehbruecke, Germany[a]; IFOM (Foundation FIRC Institute of Molecular Oncology), Milan, Italy[b]; Moscow State University, Moscow, Russia[c]; Leibniz Institut für Molekulare Pharmakologie (FMP), Berlin, Germany[d]; German Center for Diabetes Research (DZD), Neuherberg, Germany[e]

The homeodomain transcription factor Prep1 was previously shown to regulate insulin sensitivity. Our aim was to study the specific role of Prep1 for the regulation of energy metabolism in skeletal muscle. Muscle-specific ablation of *Prep1* resulted in increased expression of respiratory chain subunits. This finding was consistent with an increase in mitochondrial enzyme activity without affecting mitochondrial volume fraction as assessed by electron microscopy. Metabolic phenotyping revealed no differences in daily energy expenditure or body composition. However, during treadmill exercise challenge, *Prep1* ablation resulted in a higher maximal oxidative capacity and better endurance. Elevated PGC-1α expression was identified as a cause for increased mitochondrial capacity in *Prep1* ablated mice. Prep1 stabilizes p160 Mybbp1a, a known inhibitor of PGC-1α activity. Thereby, p160 protein levels were significantly lower in the muscle of *Prep1* ablated mice. By a chromatin immunoprecipitation-sequencing (ChIP-seq) approach, PREP1 binding sites in genes encoding mitochondrial components (e.g., Ndufs2) were identified that might be responsible for elevated proteins involved in oxidative phosphorylation (OXPHOS) in the muscle of Prep1 null mutants. These results suggest that Prep1 exhibits additional direct effects on regulation of mitochondrial proteins. We therefore conclude that *Prep1* is a regulator of oxidative phosphorylation components via direct and indirect mechanisms.

Obesity can give rise to a multitude of pathological conditions collectively referred to as the metabolic syndrome. The underlying key metabolic defect is insulin resistance, which can be caused by ectopic fat storage mainly in muscle and liver (1). Skeletal muscle is the major site of oxidative glucose and lipid metabolism, and dysregulation of either of these metabolic pathways can contribute to the development of metabolic diseases such as type 2 diabetes and cardiovascular complications (2).

The *Pknox1* gene encodes the homeodomain transcription factor Prep1 that belongs to the family of TALE (three-amino-acid loop extension) proteins (3, 4). It dimerizes with Pbx proteins to increase its target specificity (5–7). Prep1, like most homeodomain factors, is also involved in the regulation of development, and consequently, deletion of Prep1 leads to embryonic lethality. However, *Prep1* hypomorphic mice (*Prep1*$^{i/i}$), which express about 2% of *Prep1* mRNA have a survival rate of 25%, whereas the remaining 75% suffer intrauterine death with developmental defects in hematopoiesis, oculogenesis, and angiogenesis (8). Using the *Prep1* hypomorphic mouse model, it was recently reported that Prep1 is involved in the regulation of glucose metabolism (9). *Prep1* hypomorphic mice were shown to be more insulin sensitive than wild-type animals, and it was concluded that this was due to increased GLUT4-mediated glucose uptake in skeletal muscle (9). *Prep1* hypomorphic mice have other phenotypes relevant to systemic glucose metabolism such as changes in beta-cell proliferation (9), enhanced hepatic insulin responsiveness, and reduced hepatic glucose output (10). Therefore, we ablated *Prep1* specifically in skeletal muscle in order to test the hypothesis that Prep1 is involved in the regulation of energy metabolism in skeletal muscle.

MATERIALS AND METHODS

Animal studies. Animals were kept in a temperature-controlled room (22 ± 1°C) on a 12-h light/dark cycle with free access to food and water. All animal studies were conducted in accordance with the NIH guidelines for the care and use of laboratory animals (11), and all experiments were approved by the ethics committee of the State Agency of Environment, Health and Consumer Protection (State of Brandenburg, Germany).

Generation of *Prep1* hypomorphic and *Prep1*-loxP mice was described elsewhere (8, 12). Briefly, *Prep1* hypomorphic mice have a retroviral vector (VICTR45) inserted into intron 1, and *Prep1*-loxP mice have loxP sites flanking exons 6 and 7 of the *Prep1* gene. Genotyping of the mice was performed by genomic PCR on DNA isolated from tail biopsy specimens) (Fig. 1A, primers A to E). The primers and primer sequences used were as follows: primer A, GGCACATCGTGAAGTTGGG; primer B, GCAGGTTAGAAAGGGAGGAC; primer C, CCAAGGGCAGTAAGAGAAGCTCTGCAG; primer D, CAAAATGGCGTTACTTAAGCTAGCTTGCC; and primer E, GGAGTGCCAACCATGTTAAGAAGAAGTCCC. All three mouse lines (*Prep1*$^{f/f}$, *Prep1*$^{i/i}$, and MCK-Cre) were backcrossed to C57BL/6 mice for at least 10 generations to minimize variation due to differences in genetic background.

Body composition was analyzed weekly by nuclear magnetic resonance (NMR) (Minispec LF50; Bruker Biospin Corporation, Billerica, MA, USA). Energy expenditure and respiratory quotient were measured by indirect calorimetry as described elsewhere (13).

For assessment of glucose tolerance, animals were not fed for 6 h, and then they received intraperitoneal (i.p.) injection of 2 mg of glucose/g of body weight. For insulin tolerance tests (ITT), food was withdrawn for 1 h, and then the mice received 0.75 mU of insulin/g of body weight i.p. (Actrapid; Novo Nordisk, Mainz, Germany). For glucose tolerance tests only, blood sugar was measured in blood samples taken from the tail 15,

Received 17 September 2013 Returned for modification 4 October 2013
Accepted 5 November 2013
Published ahead of print 11 November 2013
Address correspondence to Timo Kanzleiter, Kanzleiter@dife.de.

doi:10.1128/MCB.01232-13

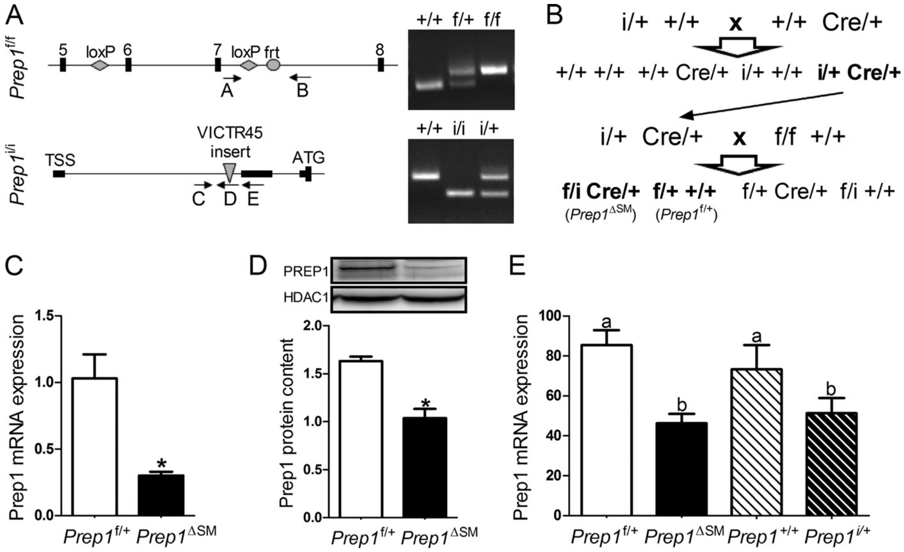

FIG 1 Efficiency of *Prep1* ablation in $Prep1^{\Delta SM}$ mice. (A) Genomic organization and genotyping strategy for $Prep1^{f/f}$ and $Prep1^{i/i}$ mice. Primers A to E for genomic PCR are shown in Materials and Methods. Exons 5 to 8, the FLP recombination target (frt), and transcriptional start site (TSS) are shown. (B) Breeding scheme for double heterozygous *Prep1* mice (i, *Prep1* hypomorphic allele; f, *Prep1*-loxP allele; Cre, Cre recombinase). (C) *Prep1* mRNA levels were measured in tibialis muscle of 8-week-old male $Prep1^{f/+}$ and $Prep1^{\Delta SM}$ mice and expressed in relation to $Prep1^{f/+}$ mice. (D) PREP1 protein levels were detected in nuclear extracts of tibialis muscle (from 8-week-old mice) and normalized to histone deacetylase 1 (HDAC1) levels. (E) Prep1 expression in heart muscle for *Prep1* double heterozygous ($Prep1^{\Delta SM}$) and hypomorphic ($Prep1^{i/+}$) mice. (Bars with the same letters are not significantly different; $P < 0.05$ by analysis of variance [ANOVA]; 4 to 15 mice/group). Data points are means plus standard errors (error bars). Values that are significantly different ($P < 0.05$) from the value for $Prep1^{f/+}$ mice by Student's *t* test are indicated by an asterisk (5 to 8 mice/group).

30, 60, and 120 min after injection. For random blood glucose measurements, animals were measured in the morning without food withdrawal.

The maximal oxidative capacity and endurance of the mice were measured on an airtight metabolic treadmill (Columbus Instruments, Columbus, OH, USA) connected to an Oxymax oxygen and carbon dioxide analyzer (Columbus Instruments, Columbus, OH, USA). The animals were running on a 20° incline, and the treadmill speed was increased by 2 m/min every 2 min. The treadmill was stopped if any of the following conditions was met. (i) The mice refused to run any further and remained on the shock grid for more than 5 s. (ii) The oxygen consumption did not increase any further after increase of the treadmill speed. (iii) The respiratory quotient rose rapidly over 1, indicating anaerobic conditions.

Mitochondrial properties. Mitochondrial density was assessed by quantitative PCR (qPCR) amplification of genomic DNA (glucagon) and mitochondrial DNA (mtDNA) (cytochrome *b*) in isolated DNA from tibialis anterior muscle. The ratio of relative abundance values between mtDNA and genomic DNA was used as an indicator of mitochondrial density.

For measurement of citrate synthase activity, frozen muscle samples were homogenized in Tris-EDTA buffer (pH 7.4), and cleared supernatant after centrifugation was used for a spectrophotometric assay. The conversion rate of acetyl coenzyme A (acetyl-CoA) and oxaloacetate to citrate and CoA-SH by citrate synthase is proportional to the coupled reaction of CoA-SH and 5,5′-dithiobis(2-nitrobenzoic acid) (DTNB; Sigma-Aldrich) to 2-nitro-5-thiobenzoate (NTB), which was measured at 412 nm.

RNA and protein analyses. For cells and tissue samples, RNA was isolated according to the manufacturer's instructions using TRI reagent (Sigma-Aldrich). RNA integrity was measured on LabChips in an Agilent bioanalyzer, and RNA concentration was determined spectrophotometrically using a Nanodrop spectrophotometer (Thermo Scientific). For conversion into cDNA, random primers and the cDNA synthesis kit from Qiagen were used. Quantitative real-time PCR was performed on Roche Lightcycler 480 using gene-specific primers and corresponding universal probe library (UPL) probes (Roche) (Table 1). For muscle samples, the eukaryotic translation elongation factor 2 (Eef2) was used as an endogenous control. Transcriptional profiling of muscle samples was performed on Agilent 4×44K whole-genome microarrays by SourceBioSciences (Berlin). Array results were analyzed by gene set enrichment using the MetaCore database (Thomson Reuters).

For immunoblot analysis, frozen muscle samples were powdered and solubilized in radioimmunoprecipitation (RIPA) buffer supplemented with protease and phosphatase inhibitors (Roche). Protein concentration was measured in cleared supernatants using the bicinchoninic acid (BCA) assay (Pierce). Protein (30 μg) was diluted in Laemmli SDS buffer and separated on an SDS gel. After transfer to a polyvinylidene fluoride (PVDF) membrane, antibodies against Prep1 (sc-6245; Santa Cruz), PGC-1α (Cell Signaling), p160 c-myb binding protein 1 (Mybp1) (Invitrogen), glyceraldehyde-3-phosphate dehydrogenase (GAPDH) (Ambion), alpha-tubulin (Sigma-Aldrich), and MitoProfile total OXPHOS rodent WB antibody cocktail (MitoSciences) were used for the immunodetection of respective proteins.

Electron microscopy. Mice were transcardially perfused with 2% paraformaldehyde–2.5% glutaraldehyde. Tibialis anterior (TA) muscles were isolated and postfixed in the same fixative for 1 day. TA muscles were washed and cut longitudinally to strips that were 0.5 mm thick. Following osmification with 2% osmium tetroxide and 1% uranyl acetate *en bloc*, staining tissue was routinely dehydrated in methanol gradient solutions and embedded in epoxy resin. After polymerization, median regions of the muscle were trimmed for subsequent ultramicroscopic analysis. Images were taken with a Technai transmission electron microscope at a magnification of ×3,500 using a Gatan charge-coupled-device (CCD) camera. Multiple images were combined in order to reconstruct an area of ≈16 by 16 μm per each muscle fiber analyzed. Images from 25 individual muscle fibers and 3 animals per genotype were analyzed. Mitochondrial volume fraction was estimated by superimposing a grid over an image of muscle fiber and getting a ratio of crossings targeting mitochondria over the total number of crossings targeting a muscle fiber.

ChIP assay. Chromatin immunoprecipitations (ChIPs) were performed using standard methods as described elsewhere (7) on differenti-

TABLE 1 PCR primers and corresponding UPL probes[a]

Gene	Primer sequence: Forward (5′–3′)	Primer sequence: Reverse (5′–3′)	UPL probe or dye
Ndufs2	AGGAAACAGCCCACTGGAA	ATGTTGGTCACCGCTTTTTC	63
Ndufa10	GGACATCGAGAATGCGTACA	TCGTACACCAACACCTCACAC	69
Sdha	TGTTCAGTTCCACCCCACA	TCTCCACGACACCCTTCTG	71
Cyc1	TGCTACACGGAGGAAGAAGC	CCATCATCATTAGGGCCATC	10
Cox5a	TTAAATGAATTGGGAATCTCCAC	GTCCTTAGGAAGCCCATCG	17
Atp5k	CTAAAACCCCGGGCAGAG	GAGAATGCTGTCATCTTGAGCTT	55
Cytc	CATTTATTATCGCGGCCCTA	TGTTGGGTTGTTTGATCCTG	SYBR green
Gluc	CAGGGCCATCTCAGAACC	GCTATTGGAAAGCCTCTTGC	SYBR green
Serca1	AAGGCTCGGGACATCGTT	GGATGTCTGCAGGGACTTTG	10
Serca2	CCATGAGCAAGATGTTTGTGA	ATGGGGACCTTGGTACTTCC	50
Tnni1	GCCGGAAGTTGAGAGGAAAT	CCTGCTCCCAACACTCCTT	16
Tnni2	AGGTGAAGGTGCAGAAGAGC	TTGCCCCTCAGGTCAAATAG	17

[a] UPL, universal probe library.

ated C2C12 myotubes. We used anti-Prep1 antibody for immunoprecipitation of sheared chromatin fragments. Enrichment for Prep1 binding in immunoprecipitated chromatin was tested by standard endpoint PCR (30 cycles) as well as qPCR using SYBR green.

Microarray data accession number. Microarray data were deposited at Gene Expression Omnibus and assigned accession number GSE52424.

RESULTS

Generation of double heterozygous *Prep1 MCK-Cre* mice. In a first approach, mice with loxP sites flanking exons 6 and 7 of the *Prep1* gene (*Prep1*$^{f/f}$) (Fig. 1A) (described in reference 12) were crossed with *MCK-Cre* mice (14). The Cre-expressing offspring had Prep1 expression in skeletal muscle at a level of about 50% compared to the non-Cre-expressing mice (data not shown). In order to increase the efficiency of *Prep1* deletion, we combined the *Prep1 flox MCK-Cre* mice with *Prep1* hypomorphic mice (*Prep1*$^{i/i}$) (Fig. 1A) (8) and crossed *Prep1*$^{i/+}$ mice with heterozygous *MCK-Cre* mice and crossed the resulting *Prep1*$^{i/+\ Cre/+}$ mice with *Prep1*$^{f/f}$ mice. The double heterozygous *Prep1*$^{f/i\ Cre/+}$ offspring (from here on referred to as *Prep1*$^{\Delta SM}$) were used as a model for *Prep1* ablation and compared to *Prep1*$^{f/+\ +/+}$ mice (referred to as *Prep1*$^{f/+}$) (Fig. 1B). *Prep1*$^{\Delta SM}$ mice resulting from this breeding strategy had less than 30% of *Prep1* mRNA expression in skeletal muscle compared with *Prep1*$^{f/+}$ control mice (Fig. 1C). PREP1 protein levels were significantly reduced to about 60% of *Prep1*$^{f/+}$ control mice (Fig. 1D). Since the MCK promoter is also active in heart, we studied the expression of Prep1 in this organ and detected a 45% reduction in *Prep1*$^{\Delta SM}$ mice (Fig. 1E).

***Prep1* is a negative regulator of respiratory chain subunits.** In order to identify target genes that are affected by *Prep1* ablation, transcriptional profiling was performed. Therefore, isolated RNA from tibialis muscle of 8-week-old male *Prep1*$^{\Delta SM}$ and *Prep1*$^{f/+}$ mice was hybridized to Agilent microarrays. This revealed 1,384 differentially expressed genes ($P < 0.05$) in response to *Prep1* ablation. Gene enrichment analysis (Metacore database) revealed a significant enrichment of differentially expressed genes involved in oxidative phosphorylation (OXPHOS) ($P = 0.009$). This included subunits from all five complexes of the respiratory chain. Validation of the microarray results confirmed significantly increased expression of succinate dehydrogenase subunit (*Sdha*) from complex 2, cytochrome c_1 subunit (*Cyc1*) from complex 3, and ATP synthase subunit (*Atp5k*) from complex 5 in *Prep1* ablated muscles. The NADH dehydrogenase subunit (*Ndufa10*; complex 1) displayed a trend ($P = 0.059$) toward increased expression (Fig. 2A). To further analyze enzymes involved in oxidative phosphorylation, we performed immunoblotting for OXPHOS components and observed significantly increased protein content for complex 1 (Ndufb8), complex 2 (Sdhb), complex 4 (Mtco1), and complex 5 (Atp5a) (Fig. 2B).

Altered mitochondrial properties in muscle of *Prep1* ablated mice. In order to test whether increased OXPHOS proteins are a consequence of elevated mitochondrial number, we measured mitochondrial DNA by mitochondrial qPCR (mito-qPCR) and found significantly increased amounts of mtDNA in muscle of *Prep1* ablated mice (Fig. 3A). In line with this finding was an in-

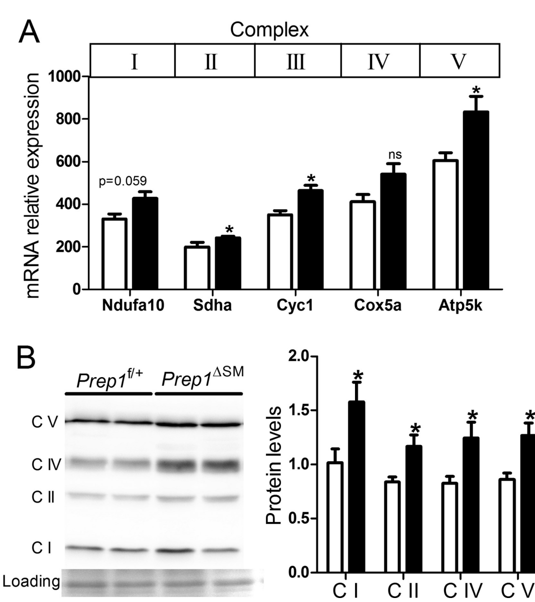

FIG 2 Expression of respiratory chain subunits in *Prep1*$^{\Delta SM}$ mice. (A) Subunits of complexes I to V in the respiratory chain that were differentially expressed as detected by microarray analysis were validated by qPCR. (B) Protein levels of subunits from *Prep1*$^{\Delta SM}$ muscle samples. Subunits of complex I (C I) to complex V (C V) from muscle samples from *Prep1*$^{f/+}$ mice (white bars) and *Prep1*$^{\Delta SM}$ mice (black bars) are shown. Data are presented as means plus standard errors. Values that are significantly different ($P < 0.05$) from the value for *Prep1*$^{f/+}$ mice by Student's *t* test are indicated by an asterisk or by the *P* value (10 to 14 mice/group). ns, not significant.

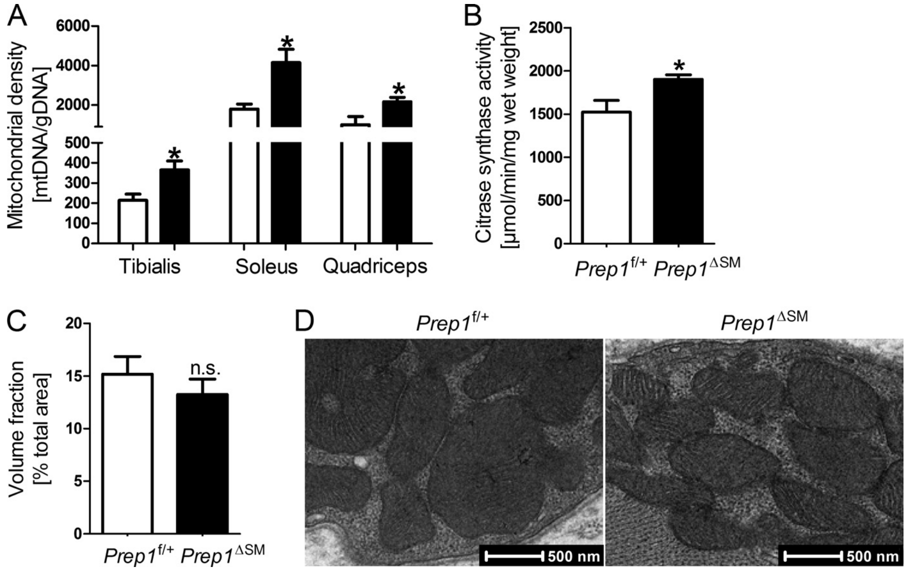

FIG 3 Mitochondrial properties of *Prep1*$^{\Delta SM}$ mice. (A) Mitochondrial density in different muscle groups was assessed by the ratio of mitochondrial DNA (mtDNA; cytochrome *b*) and genomic DNA (gDNA; glucagon) (6 to 9 mice/group). The muscle samples were from *Prep1*$^{f/+}$ mice (white bars) and *Prep1*$^{\Delta SM}$ mice (black bars). (B) Activity of the mitochondrial enzyme citrate synthase was measured in tibialis muscle homogenates as described in Materials and Methods (8 mice/group). (C) Mitochondrial volume fraction was measured in ultrathin tibialis muscle sections with electron microscopy (EM). (D) Mitochondrial ultrastructure in *Prep1*$^{\Delta SM}$ mice. Data points are means plus standard errors. Values that are significantly different ($P < 0.05$) from the value for *Prep1*$^{f/+}$ mice by Student's *t* test are indicated by an asterisk. n.s., not significant.

creased activity of the mitochondrial enzyme citrate synthase in *Prep1* ablated animals, supporting our assumption of enhanced mitochondrial properties in the absence of *Prep1* (Fig. 3B). However, studies by electron microscopy did not show an increased mitochondrial volume fraction (Fig. 3C) or changes in the ultrastructure of mitochondria between control and *Prep1*$^{\Delta SM}$ mice (Fig. 3D).

Metabolic phenotyping of *Prep1* ablated mice. To investigate possible metabolic consequences of altered mitochondrial properties, body weight and composition were measured weekly in mice kept on a standard diet over a period of 24 weeks. However, no differences in body weight or composition were detected (Fig. 4B). Whole-body energy expenditure and respiratory quotient of these animals determined by indirect calorimetry in either the dark or light phase were not different from those of control mice (Fig. 4A). Possible consequences of *Prep1* ablation in muscle on the regulation of glucose metabolism were investigated by measuring random blood glucose levels and by testing insulin and glucose tolerance (at week 8 and 9, respectively). Blood glucose levels were unaffected (data not shown), and the animals exhibited no differences in insulin or glucose tolerance (Fig. 4C and D). The reason for this might be the fact that the levels of GLUT4 expression were unchanged in *Prep1*$^{f/+}$ and *Prep1*$^{\Delta SM}$ mice in tibialis muscle in contrast to wild-type and *Prep1*$^{i/i}$ mice (Fig. 4E).

Maximal oxidative capacity and endurance. Given the increased amount of respiratory chain subunits, we hypothesized that the *Prep1*$^{\Delta SM}$ mice might show metabolic differences after exercise challenge. Therefore, oxygen consumption was measured during forced treadmill running until exhaustion to measure the peak oxygen consumption (VO_2 peak). Interestingly, the maximal oxidative capacity was significantly higher in the *Prep1*$^{\Delta SM}$ mice compared to the controls (Fig. 5A). In addition, *Prep1* ablated mice also performed better and did run a longer distance until exhausted compared to their control littermates (Fig. 5B).

Maximal oxidative capacity and endurance are also influenced by heart function, and as mentioned above, *Prep1*$^{\Delta SM}$ mice do have decreased expression of Prep1 in the heart (Fig. 1E). Therefore, we used heterozygous *Prep1* hypomorphic mice (*Prep1*$^{i/+}$) with comparable expression of Prep1 (Fig. 1E) in the heart but significantly more Prep1 expression in muscle (~2.5-fold) to evaluate a possible contribution of heart function. *Prep1*$^{i/+}$ mice did not have a significantly different maximal oxidative capacity or changes in endurance capacity (Fig. 5A and B).

The fiber type composition of the muscle can also have a great influence on endurance and oxidative capacity, and therefore, we measured fiber type-specific isoforms of sarco/endoplasmic reticulum Ca^{2+}-ATPase 1 and 2 (Serca1 and Serca2, respectively) and troponins 1 and 2. There was not a difference in Serca2 and troponin 1, which are predominantly expressed in type 1 fibers, or in Serca1 and troponin 2, which are mainly found in type 2 fibers (Fig. 5C).

PREP1 affects PGC-1α activity. The molecular mechanism behind the altered mitochondrial properties in *Prep1* ablated animals was investigated by measuring regulators of mitochondrial metabolism. The coactivator PGC-1α is well-known as a central regulator of mitochondrial metabolism and showed increased expression in our microarray analysis (Fig. 6A). Consistent with the increase in PGC-1α mRNA, we also found protein levels to be significantly increased in the muscle of *Prep1*$^{\Delta SM}$ mice compared to control mice (Fig. 6B). The activity of PGC-1α depends on the stability of p160 Mybp1 (p160 c-myb binding protein 1; p160), which is a known inhibitor of PGC-1α (15). PREP1 interacts with p160 to protect it from proteasomal degradation (16). Immunoblotting of muscle lysates revealed p160 levels to be significantly decreased in muscle of *Prep1*$^{\Delta SM}$ mice (Fig. 6C), thereby supporting the hypothesis that the increased degradation of p160 indirectly increases PGC-1α activity (Fig. 7C). To test whether increased PGC-1α levels modulate expression of transcription

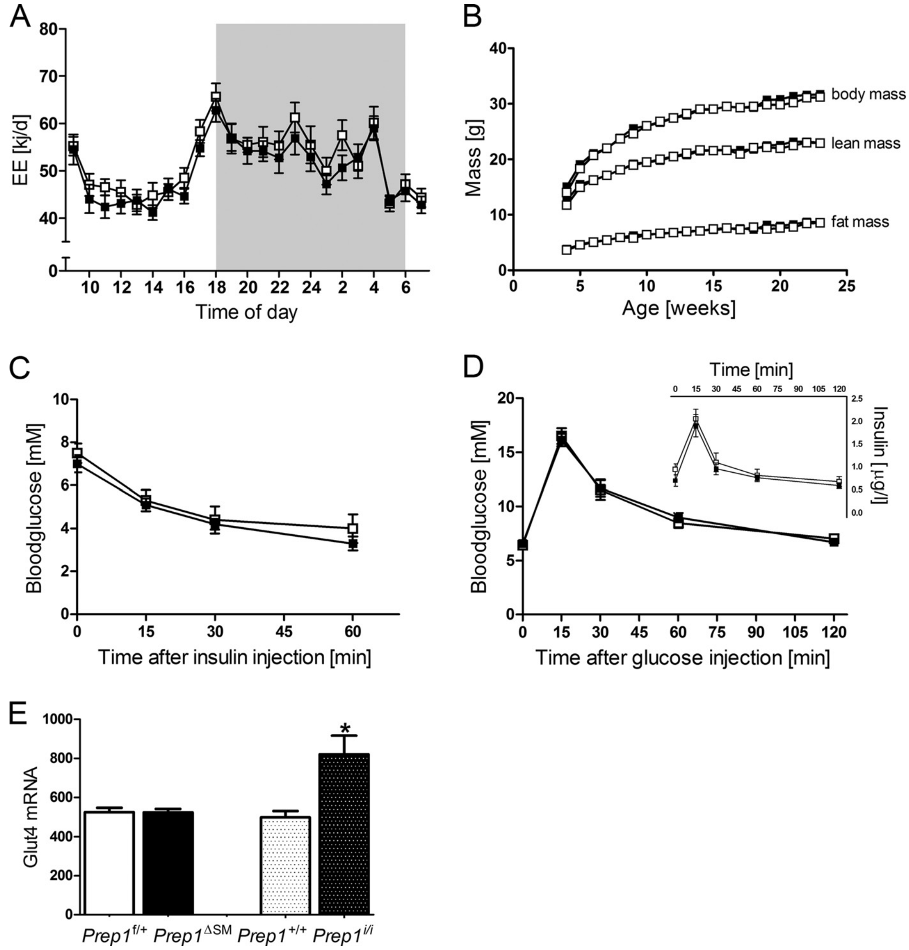

FIG 4 Metabolic phenotyping of *Prep1*$^{\Delta SM}$ mice. (A) Daily energy expenditure (EE) (in kilojoules per day [kj/d]) was measured by indirect calorimetry in 16-week-old male mice (12 to 14 mice/group). The time of day is shown in hours with the light (white background) and dark (gray background) portions of the light/dark cycle indicated. (B) Body composition was measured weekly by NMR (11 to 32 mice per group per time point). (C and D) Insulin (C) and glucose (D) tolerance was measured in 8- or 9-week-old male mice (10 mice/group) as described in Materials and Methods. Insulin levels (in micrograms per liter) for the glucose tolerance test are shown in the inset in panel D. In panels A to D, the mean ± standard error values for *Prep1*$^{f/+}$ mice (white squares) and *Prep1*$^{\Delta SM}$ mice (black squares) are shown. (E) Glut4 mRNA was measured by qPCR in tibialis muscle of *Prep1*$^{f/+}$, *Prep1*$^{\Delta SM}$, and Prep1 hypomorphic mice (*Prep1*$^{i/i}$ and wild-type littermates *Prep1*$^{+/+}$). The value that is significantly different ($P < 0.05$) from the value for *Prep1*$^{+/+}$ mice by Student's *t* test is indicated by an asterisk.

factors that regulate mitochondrial biogenesis, we studied expression of nuclear respiratory factor (NRF) (NRF1 and -2), Tfam, estrogen-related receptor (ERR) (ERRα, -β, and -γ), peroxisome proliferator-activated receptor (PPAR) (PPARα, -δ, and -γ), and liver X receptor (LXR) (LXRα and -β) known to be coactivated by PGC-1α. As shown in Fig. 6D, no significant differences in the expression of these candidates were visible in *Prep1*$^{\Delta SM}$ mice.

Prep1 directly regulates mitochondrial proteins by binding to the promoter regions of their genes. The indirect effect of Prep1 on mitochondrial components via the p160–PGC-1α pathway does not exclude the possibility that Prep1 also directly affects expression of mitochondrial proteins. Direct targets of Prep1 as previously identified by chromatin immunoprecipitation-sequencing (ChIP-seq) analysis in embryonic day 11.5 (E11.5) mouse trunk embryos (7) (GSE39609) were compared to differentially expressed genes in *Prep1*$^{\Delta SM}$ mice. This revealed 259 genes with PREP1 binding sites in their promoter region that were differentially expressed in skeletal muscle of *Prep1*$^{\Delta SM}$ mice. Gene enrichment analysis identified mitochondrial components (Gene Ontology accession number GO:0005739~mitochondrion) with 16 of the 259 genes as the most enriched category ($P = 9.08E-05$) (Table 2). Among the 16 genes with mitochondrial function were genes encoding enzymes of the tricarboxylic acid (TCA) cycle (*Ogdh*), proteins from complex 1 in the respiratory chain (*Ndufs2*), and genes involved in heme biosynthesis (*Isca1*), transport across membranes (*Abcf2*), and a novel inhibitor of IRS1 signaling (*Macrod1*) (Table 2). Binding of PREP1 to the promoters of these genes was validated by ChIP in C2C12 muscle cells (Fig. 7A and B). This suggests that Prep1 directly binds to the gene regulatory region of mitochondrial components and thereby inhibits their expression.

DISCUSSION

Our results from muscle-specific deletion of *Prep1* demonstrate its important role for the regulation of the OXPHOS system with the consequence of improved maximal oxidative capacity and endurance during exercise challenge. First, we show that *Prep1* ablation in muscle leads to an increase in mRNA and protein abundance of

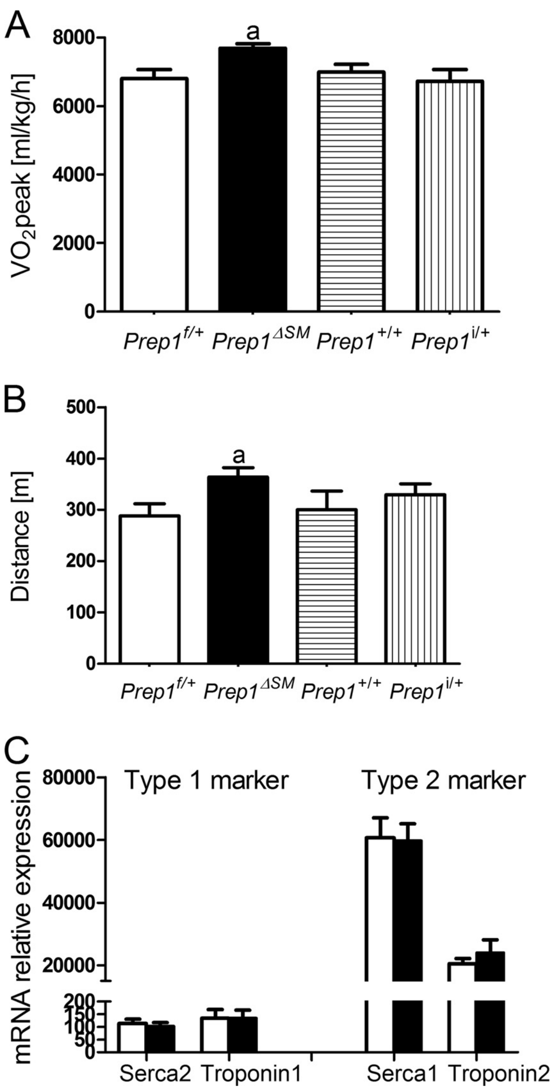

FIG 5 *Prep1* ablation results in increased maximal oxidative capacity and endurance. (A) Maximal oxidative capacity of 14-week-old female mice (9 to 12 mice/group) was measured on an airtight motorized treadmill. (B) Maximal running distance till exhaustion during an exercise challenge on a motorized treadmill (9 to 12 mice/group). (C) Muscle fiber type composition was determined by measurement of fiber type-specific isoforms of Serca and troponin in tibialis muscle samples. All data presented are means plus standard errors, and statistical significance was tested with ANOVA and *post hoc* pairwise comparison (values that are significantly different [$P < 0.05$] from the values for all other genotypes are indicated by the letter a).

mitochondrial OXPHOS proteins from all complexes of the respiratory chain and an increased citrate synthase activity. These changes had no consequences for whole-body energy expenditure of the mice. This somewhat counterintuitive finding is easily explained by the huge capacity of skeletal muscle to increase oxidation of energy substrates above resting levels. Skeletal muscle contains enough mitochondria to increase maximal oxygen uptake during exercise by 150-fold in young trained men, and even for untrained sedentary men, the increase was estimated to be 30- to 40-fold (17, 18). Whole-body energy expenditure is usually measured during periods of rest and light activity, conditions that would not show differences due to increased mitochondrial capacity. With no changes in daily energy expenditure, it is also not surprising that body weight and composition were unchanged in *Prep1*$^{\Delta SM}$ mice. However, under challenging conditions of treadmill exercise, maximal oxygen consumption in *Prep1* ablated animals was significantly increased, presumably due to an increased muscular mitochondrial capacity. This resulted in higher endurance as indicated by the longer distance run by *Prep1*$^{\Delta SM}$ mice. Contribution of altered Prep1 expression in the heart can be excluded as a cause for augmented maximal oxidative capacity, since we found no changes in VO_2 peak in heterozygous *Prep1* hypomorphic mice (Fig. 5A), which display a Prep1 expression level in the heart that is similar to that in *Prep1*$^{\Delta SM}$ mice (Fig. 1E).

Impaired mitochondrial function is intensively discussed as a possible mechanism underlying insulin resistance. Over a decade ago, it was shown for the first time that muscle of type 2 diabetics and obese individuals contains less mitochondria than those of insulin-sensitive individuals (19, 20). This gave rise to the popular theory that the decreased ability to oxidize fat in muscle would lead to accumulation of lipid species and impede insulin action (21). However, it has not yet been resolved whether mitochondrial dysfunction is cause or consequence of insulin resistance (22). One could assume that an increased capacity to oxidize fat could be very beneficial to overcome insulin resistance as long as this increased mitochondrial capacity is used. The increase in OXPHOS components of *Prep1*$^{\Delta SM}$ mice did not result in improved glucose uptake and insulin action under standard-diet conditions. However, it is tempting to speculate that *Prep1* deficiency may retain insulin sensitivity when mice are challenged by increased energy intake (e.g., high-fat feeding). Results from our insulin tolerance tests (ITT) are in contrast to the findings of Oriente and colleagues who reported an increased response to insulin during ITT in *Prep1* hypomorphic mice (9). One possible explanation for this discrepancy is effects of *Prep1* ablation in nonmuscle tissues. Indeed, it was reported that *Prep1* hypomorphic mice show a decreased hepatic glucose output and have decreased glucagon levels in plasma (10) that might contribute to increased insulin responsiveness during an ITT. Another explanation for this discrepancy might be different effects on GLUT4 levels in the two *Prep1* mouse models. Whereas *Prep1* hypomorphic mice show a significant increase in Glut4 expression in tibialis muscle, there is no effect on GLUT4 to be seen in our *Prep1*$^{\Delta SM}$ mice (Fig. 4E).

How does Prep1 regulate expression of OXPHOS proteins? A well-known regulator of muscle oxidative capacity is the transcriptional coactivator PGC-1α, which we found to be significantly upregulated in *Prep1* ablated muscle. ChIP-seq analysis did not identify PGC-1α as a direct target of Prep1, suggesting that PGC-1α is most likely indirectly regulated. Prep1 cannot only dimerize with Pbx transcription factors and directly bind to DNA (5), it was also shown to interact with p160 Mybbp1a (16). This dimerization protects p160 from proteasomal degradation (9). Interestingly, p160 is a known repressor of PGC-1α activity (15). Thus, we speculated that p160 is degraded in muscle of *Prep1*$^{\Delta SM}$ mice, which blocks the inhibition of PGC-1α, finally resulting in elevated expression of mitochondrial components. Actually, we observed a decrease in p160 protein content in *Prep1* ablated muscles and the resulting increase of PGC-1α protein content. This confirms the findings of Oriente and colleagues who described a p160-dependent regulation of PGC-1α by Prep1 in *Prep1* hypomorphic mice (9).

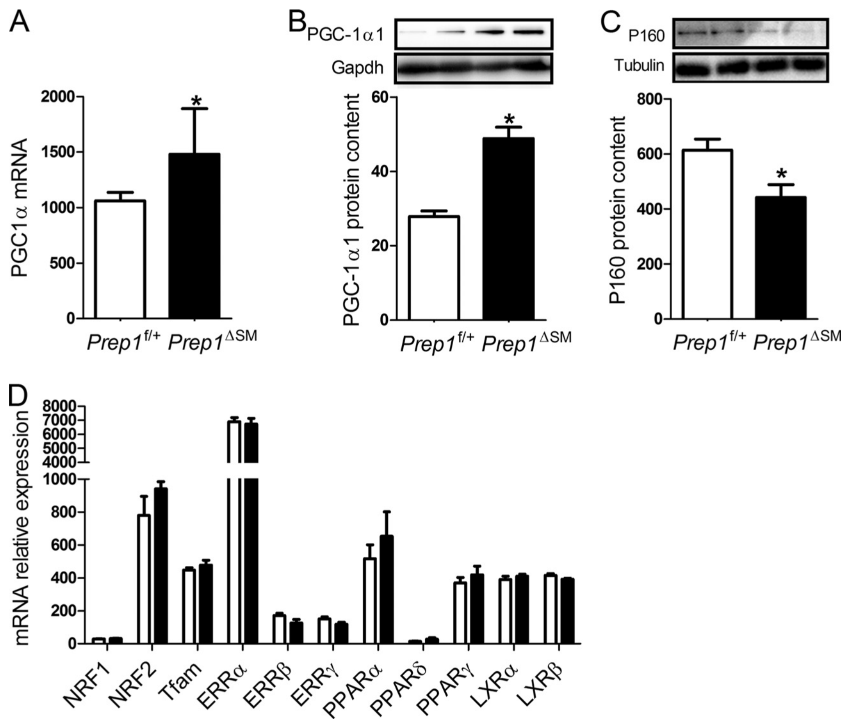

FIG 6 *Prep1* ablation activates the p160–PGC-1α pathway. (A and B) PGC-1α mRNA expression was found to be increased in response to *Prep1* ablation as detected by microarray analysis (4 mice/group) (A), and this translated into higher PGC-1α protein levels (7 mice/group) (B). (C) p160 protein levels were reduced in muscle of *Prep1*$^{\Delta SM}$ mice (7 mice/group). (D) Known regulators and interaction partners of PGC-1α were measured by qPCR in tibialis muscle of *Prep1*$^{f/+}$ and *Prep1*$^{\Delta SM}$ mice. In panels A to D, the values for *Prep1*$^{f/+}$ mice (white bars) and *Prep1*$^{\Delta SM}$ mice (black bars) are shown. All data presented are means plus standard errors. Values that are significantly different ($P < 0.05$) from the value for *Prep1*$^{f/+}$ mice by Student's *t* test are indicated by an asterisk.

However, this does not exclude the possibility that *Prep1* also has additional direct effects on the expression of mitochondrial proteins. Interestingly, ChIP-seq identified PREP1 binding sites in the promoter regions of genes encoding 16 mitochondrial proteins that were also differentially expressed in skeletal muscle in response to *Prep1* ablation. This suggests that Prep1 is a direct negative transcriptional regulator of mitochondrial proteins in addition to its indirect effects via p160–PGC-1α. Most interesting is the Prep1 binding site in the *Ndufs2* gene, which is part of complex 1 in the OXPHOS system. This exemplifies direct effects of Prep1 on the OXPHOS system by demonstrating PREP1 binding to a complex 1 subunit gene in muscle cells as well as increased mRNA and protein abundance for complex 1 in response to Prep1 ablation. Another interesting finding is the Prep1 binding site in

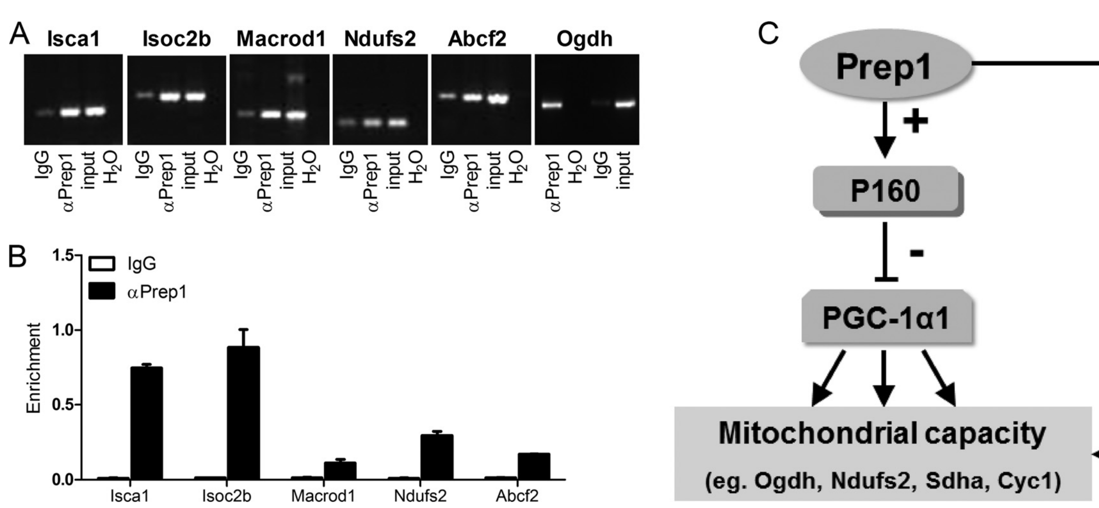

FIG 7 Prep1 binding sites in muscle cells. (A) ChIP-seq results were validated in single ChIP experiments in C2C12 muscle cells. Endpoint PCR revealed enrichment of promoter regions in samples immunoprecipitated with anti-Prep1 antibody (αPrep1). (B) Quantitative real-time PCR confirmed the enrichment in αPrep1 samples. (C) Proposed mechanism of how Prep1 influences mitochondrial capacity indirectly via the p160–PGC-1α pathway and directly as a negative transcriptional regulator.

TABLE 2 Putative mitochondrial Prep1 targets

			RT-PCR[c]		ChIP-seq		
RefSeq ID[a]	Gene[b]	Microarray ratio[d]	Ratio[d]	*P* value[b]	Score	Distance to TSS[e] (bp)	FDR[f] (%)
NM_153082	*Dnajc27*	1.40	1.05	0.61908	3,100	−427	0
NM_026921	***Isca1***	1.22	1.15	**0.04682**	3,100	−53	0
NM_010956	***Ogdh***	1.29	2.81	**0.02728**	3,100	−317	0
NM_144801	*Tmem143*	1.35	0.96	0.17733	902	−4,733	0.11
NM_025460	*Tmem126a*	1.17	0.88	0.05947	785	−18,780	0.12
NM_026938	*Tmem160*	0.95	0.87	0.11775	1,901	−244	0.17
NM_025570	*Mrpl20*	0.93	1.26	0.08705	3,140	−8,758	0.18
NM_017393	*Clpp*	0.91	1.15	0.26435	1,347	−6,997	0.2
NM_013853	***Abcf2***	1.30	1.13	**0.02682**	1,702	−9,255	0.25
NM_153064	***Ndufs2***	1.45	2.09	**0.03669**	293	−3,268	0.31
NM_007744	*Comt*	0.89	1.01	0.99243	225	−2,226	22.55
NM_024274	*Fars2*	1.29	1.09	0.25118	111	−57,908	33
NM_023231	*Stoml2*	1.24	0.85	0.10076	370	−119	37
NM_008301	*Hspa2*	0.74	0.97	0.77133	3,100	120	ND
NM_134147	***Macrod1***	0.86	0.88	**0.00716**	68	−1,062	ND
NM_011099	*Pkm*	1.19	1.1	0.14849	86	11	ND

[a] NCBI Reference Sequence (RefSeq) database identification (ID) or accession number.
[b] The genes that were most enriched and the corresponding *P* values are shown in boldface type.
[c] RT-PCR, reverse transcription-PCR.
[d] Ratio of *Prep1*$^{\Delta SM}$ to *Prep1*$^{f/+}$ expression values.
[e] TSS, transcriptional start site.
[f] FDR, false discovery rate.

the promoter of Ogdh, which is an enzyme of the TCA cycle. This complements the finding of increased TCA cycle activity as shown by the measurement of citrate synthase activity.

Paradoxically, the increase in mtDNA, citrase synthase activity, and OXPHOS expression we observed in *Prep1*$^{\Delta SM}$ mice was independent of mitochondrial volume fraction in muscle as assessed by electron microscopy. This is somewhat surprising given the properties of PGC-1α transgenic mice, which show robust effects on muscle fiber type switch and mitochondrial biogenesis (23). However, a noteworthy difference is the extent of PGC-1α overexpression. Whereas we have an increase of about 75% in PGC-1α protein, the transgenic mice have a much greater increase in PGC-1α protein (23). Therefore, one might speculate that a modest increase in PGC-1α does not activate mitochondrial biogenesis. Indeed, we could not find differential expression of nuclear respiratory factor 1 and 2, Tfam, ERRs, etc. (Fig. 6D), which are increased during mitochondrial biogenesis (reviewed in reference 24). In this context, a recent publication is of interest; this publication showed that a double knockout of PGC-1α and -β results in a dissociation between mitochondrial number and respiratory chain capacity (25). It is intriguing to speculate that this finding for the basal state of mitochondrial muscle function also somehow applies to our model of modest PGC-1α increase. The precise mechanism responsible for the observed dissociation between mitochondrial content and expression of OXPHOS components in our model of muscle-specific *Prep1* ablation has to be determined in further experiments.

An alternative speculative explanation could be changes in the dynamics of mitochondrial fusion. Interestingly, two factors known to regulate mitochondrial fusion, optic atrophy 1 and mitofusin 2, were significantly increased in our array analysis in response to Prep1 ablation (data not shown).

In summary, we provide evidence that establishes Prep1 as a negative regulator of OXPHOS proteins in skeletal muscle. Remarkably, this is achieved by coordinated direct and indirect regulation of mitochondrial proteins. We have shown here that Prep1 directly binds the promoter region of mitochondrial proteins, which are differentially expressed in response to *Prep1* ablation in skeletal muscle. In addition, indirect effects of Prep1 on mitochondrial proteins are mediated via a recently discovered pathway that involves dimerization of Prep1 and p160, which is thereby stabilized and can exert its inhibitory function on PGC-1α activity. The combination of direct transcriptional control and increased PGC-1α activity in response to *Prep1* ablation leads to enhanced mitochondrial capacity reflected in a higher maximal oxygen consumption and endurance.

ACKNOWLEDGMENTS

We are indebted to Malte Neubauer for expert technical assistance.

This work was supported by funding from the European Union (FP7 PREPROBEDIA), from the German Ministry of Education and Research (DZD; 01GI0922) and by the State of Brandenburg. F.B. and D. Penkov were supported by a grant from AIRC (Italian Association for Cancer Research).

REFERENCES

1. **Ravussin E, Smith SR.** 2002. Increased fat intake, impaired fat oxidation, and failure of fat cell proliferation result in ectopic fat storage, insulin resistance, and type 2 diabetes mellitus. Ann. N. Y. Acad. Sci. **967**:363–378. http://dx.doi.org/10.1111/j.1749-6632.2002.tb04292.x.
2. **Kraegen EW, Cooney GJ.** 2008. Free fatty acids and skeletal muscle insulin resistance. Curr. Opin. Lipidol. **19**:235–241. http://dx.doi.org/10.1097/01.mol.0000319118.44995.9a.
3. **Chen H, Rossier C, Nakamura Y, Lynn A, Chakravarti A, Antonarakis SE.** 1997. Cloning of a novel homeobox-containing gene, PKNOX1, and mapping to human chromosome 21q22.3. Genomics **41**:193–200. http://dx.doi.org/10.1006/geno.1997.4632.
4. **Berthelsen J, Viggiano L, Schulz H, Ferretti E, Consalez GG, Rocchi M, Blasi F.** 1998. PKNOX1, a gene encoding PREP1, a new regulator of Pbx activity, maps on human chromosome 21q22.3 and murine chromosome 17B/C. Genomics **47**:323–324. http://dx.doi.org/10.1006/geno.1997.5086.

5. **Berthelsen J, Zappavigna V, Mavilio F, Blasi F.** 1998. Prep1, a novel functional partner of Pbx proteins. EMBO J. **17:**1423–1433. http://dx.doi.org/10.1093/emboj/17.5.1423.
6. **Knoepfler PS, Calvo KR, Chen H, Antonarakis SE, Kamps MP.** 1997. Meis1 and pKnox1 bind DNA cooperatively with Pbx1 utilizing an interaction surface disrupted in oncoprotein E2a-Pbx1. Proc. Natl. Acad. Sci. U. S. A. **94:**14553–14558. http://dx.doi.org/10.1073/pnas.94.26.14553.
7. **Penkov D, San Martín DM, Fernandez-Díaz LC, Rosselló CA, Torroja C, Sánchez-Cabo F, Warnatz HJ, Sultan M, Yaspo ML, Gabrieli A, Tkachuk V, Brendolan A, Blasi F, Torres M.** 2013. Analysis of the DNA-binding profile and function of TALE homeoproteins reveals their specialization and specific interactions with Hox genes/proteins. Cell Rep. **3:**1321–1333. http://dx.doi.org/10.1016/j.celrep.2013.03.029.
8. **Ferretti E, Villaescusa JC, Di Rosa P, Fernandez-Diaz LC, Longobardi E, Mazzieri R, Miccio A, Micali N, Selleri L, Ferrari G, Blasi F.** 2006. Hypomorphic mutation of the TALE gene Prep1 (pKnox1) causes a major reduction of Pbx and Meis proteins and a pleiotropic embryonic phenotype. Mol. Cell. Biol. **26:**5650–5662. http://dx.doi.org/10.1128/MCB.00313-06.
9. **Oriente F, Fernandez Diaz LC, Miele C, Iovino S, Mori S, Diaz VM, Troncone G, Cassese A, Formisano P, Blasi F, Beguinot F.** 2008. Prep1 deficiency induces protection from diabetes and increased insulin sensitivity through a p160-mediated mechanism. Mol. Cell. Biol. **28:**5634–5645. http://dx.doi.org/10.1128/MCB.00117-08.
10. **Oriente F, Iovino S, Cabaro S, Cassese A, Longobardi E, Miele C, Ungaro P, Formisano P, Blasi F, Beguinot F.** 2011. Prep1 controls insulin glucoregulatory function in liver by transcriptional targeting of SHP1 tyrosine phosphatase. Diabetes **60:**138–147. http://dx.doi.org/10.2337/db10-0860.
11. **National Institutes of Health.** 2000. Public Health Service policy on humane care and use of laboratory animals. Office of Laboratory Animal Welfare, National Institutes of Health, Bethesda, MD.
12. **Iotti G, Mejetta S, Modica L, Penkov D, Ponzoni M, Blasi F.** 2012. Reduction of prep1 levels affects differentiation of normal and malignant B cells and accelerates myc driven lymphomagenesis. PLoS One **7:**e48353. http://dx.doi.org/10.1371/journal.pone.0048353.
13. **Schulz N, Himmelbauer H, Rath M, van Weeghel M, Houten S, Kulik W, Suhre K, Scherneck S, Vogel H, Kluge R, Wiedmer P, Joost H-G, Schürmann A.** 2011. Role of medium- and short-chain L-3-hydroxyacyl-CoA dehydrogenase in the regulation of body weight and thermogenesis. Endocrinology **152:**4641–4651. http://dx.doi.org/10.1210/en.2011-1547.
14. **Brüning JC, Michael MD, Winnay JN, Hayashi T, Hörsch D, Accili D, Goodyear LJ, Kahn CR.** 1998. A muscle-specific insulin receptor knockout exhibits features of the metabolic syndrome of NIDDM without altering glucose tolerance. Mol. Cell **2:**559–569. http://dx.doi.org/10.1016/S1097-2765(00)80155-0.
15. **Fan M, Rhee J, St-Pierre J, Handschin C, Puigserver P, Lin J, Jäeger S, Erdjument-Bromage H, Tempst P, Spiegelman BM.** 2004. Suppression of mitochondrial respiration through recruitment of p160 myb binding protein to PGC-1alpha: modulation by p38 MAPK. Genes Dev. **18:**278–289. http://dx.doi.org/10.1101/gad.1152204.
16. **Díaz VM, Mori S, Longobardi E, Menendez G, Ferrai C, Keough RA, Bachi A, Blasi F.** 2007. p160 Myb-binding protein interacts with Prep1 and inhibits its transcriptional activity. Mol. Cell. Biol. **27:**7981–7990. http://dx.doi.org/10.1128/MCB.01290-07.
17. **Andersen P, Saltin B.** 1985. Maximal perfusion of skeletal muscle in man. J. Physiol. **366:**233–249.
18. **Holloszy J.** 2009. Skeletal muscle "mitochondrial deficiency" does not mediate insulin. Am. J. Clin. Nutr. **89:**463–466. http://dx.doi.org/10.1155/2012/768304.
19. **Kelley DE, He J, Menshikova EV, Ritov VB.** 2002. Dysfunction of mitochondria in human skeletal muscle in type 2 diabetes. Diabetes **51:**2944–2950. http://dx.doi.org/10.2337/diabetes.51.10.2944.
20. **He J, Watkins S, Kelley DE.** 2001. Skeletal muscle lipid content and oxidative enzyme activity in relation to muscle fiber type in type 2 diabetes and obesity. Diabetes **50:**817–823. http://dx.doi.org/10.2337/diabetes.50.4.817.
21. **Lowell BB, Shulman GI.** 2005. Mitochondrial dysfunction and type 2 diabetes. Science **307:**384–387. http://dx.doi.org/10.1126/science.1104343.
22. **Turner N, Heilbronn LK.** 2008. Is mitochondrial dysfunction a cause of insulin resistance? Trends Endocrinol. Metab. **19:**324–330. http://dx.doi.org/10.1016/j.tem.2008.08.001.
23. **Lin J, Wu H, Tarr PT, Zhang CY, Wu Z, Boss O, Michael LF, Puigserver P, Isotani E, Olson EN, Lowell BB, Bassel-Duby R, Spiegelman BM.** 2002. Transcriptional co-activator PGC-1 alpha drives the formation of slow-twitch muscle fibres. Nature **418:**797–801. http://dx.doi.org/10.1038/nature00904.
24. **Scarpulla RC.** 2008. Transcriptional paradigms in mammalian mitochondrial biogenesis and function. Physiol. Rev. **88:**611–638. http://dx.doi.org/10.1152/physrev.00025.2007.
25. **Rowe GC, Patten IS, Zsengeller ZK, El-Khoury R, Okutsu M, Bampoh S, Koulisis N, Farrell C, Hirshman MF, Yan Z, Goodyear LJ, Rustin P, Arany Z.** 2013. Disconnecting mitochondrial content from respiratory chain capacity in PGC-1-deficient skeletal muscle. Cell Rep. **3:**1449–1456. http://dx.doi.org/10.1016/j.celrep.2013.04.023.